Multiferroic Domain Dynamics in Strained Strontium Titanate

A. Vasudevarao,[1] A. Kumar,[1] L. Tian,[1] J. H. Haeni,[1] Y. L. Li,[1,2] C.-J. Eklund,[4] Q. X. Jia,[2] R. Uecker,[3] P. Reiche,[3]
K. M. Rabe,[4] L. Q. Chen,[1] D. G. Schlom,[1] and Venkatraman Gopalan[1,*]

[1]*Department of Materials Science and Engineering, The Pennsylvania State University, University Park, Pennsylvania 16802, USA*
[2]*MPA-STC, Los Alamos National Lab, Los Alamos, New Mexico 87545, USA*
[3]*Institut für Kristallzüchtung, Max-Born-Straße 2, 12489 Berlin (Adlershof), Germany*
[4]*Department of Physics and Astronomy, Rutgers University, New Jersey 08854, USA*

Multiferroicity can be induced in strontium titanate by applying biaxial strain. Using optical second harmonic generation, we report a transition from $4/mmm$ to the ferroelectric $mm2$ phase, followed by a transition to a ferroelastic-ferroelectric $mm2$ phase in a strontium titanate thin film. Piezoelectric force microscopy is used to study ferroelectric domain switching. Second harmonic generation, combined with phase-field modeling, is used to reveal the mechanism of coupled ferroelectric-ferroelastic domain wall motion. These studies have relevance to multiferroics with coupled polar and axial phenomena.

Multiferroic materials with multiple order parameters are attracting significant interest due to the possibility of a rich array of coupled phenomena such as ferroelastic-electric-magnetic, piezoelectric-magnetic, and electromagneto-optic effects [1–3]. At first glance, strontium titanate would appear an unlikely candidate for a multiferroic. Bulk SrTiO$_3$ is a cubic ($m\bar{3}m$) centrosymmetric perovskite at room temperature; it undergoes a nonpolar antiferrodistortive (AFD) phase transformation to a tetragonal point group $4/mmm$ at ~ 105 K and exhibits indications of a frustrated ferroelectric (FE) transition at ~ 20 K, which it never completes [4]. First principles calculations [5] and thermodynamic analysis [6,7] have suggested, however, that external strain can induce ferroelectricity. This prediction has been experimentally confirmed recently in a SrTiO$_3$ thin film strained in biaxial tension [8]. The multiferroic nature of strained strontium titanate, i.e., the coexistence of ferroelectric and ferroelastic domains, is unique in many respects. It is induced by external strain. Further, unlike other ferroelectric-ferroelastics, two independent primary order parameters exist: a polar ferroelectric order parameter **p** and an axial antiferrodistortive rotation order parameter **q** [7,9–11]. Hence, depending on the strain, the ferroelectric transition temperature can precede or succeed the ferroelastic transition temperature [7]. From a symmetry perspective, the SrTiO$_3$ multiferroic domain structure has striking similarities with, and, hence, of broader relevance to, other multiferroics with coexisting polar and axial phenomena, such as materials that exhibit coexisting ferroelectricity (polar property) and antiferromagnetism (axial property) [3,12].

This Letter focuses on the domain structure and phase transitions in a 500 Å thick SrTiO$_3$ thin film grown on a (110) DyScO$_3$ substrate with a 0.94% uniform in-plane biaxial tensile strain in the growth plane [8]. (This is the same film that was studied by Haeni *et al.* in Ref. [8].) Thermodynamic calculations predict a FE transition temperature range of 277 ± 100 K and an AFD transition at ~ 111–150 K [7,13]. First principles calculations were performed for this strain value with an $Amm2$ space group symmetry in the FE phase and an $Ima2$ (No. 46) symmetry in the multiferroic (FE + AFD) phase. In the multiferroic phase, the optimized ground state structure has a ferroelectric polarization of **p** ~ 0.18 C/m^2 in the $\langle 110 \rangle_p$ direction in the growth plane and a corresponding antiferrodistortive rotation of the oxygen octahedra by $5.9°$ about the vector **q**$\langle 110 \rangle_p$, where the subscript p refers to the pseudocubic Miller index, showing that the combination of the two distortions is lower in energy than either distortion alone. In this phase, there are 8 types of coexisting FE + AFD domains [see Fig. 1(d)], which we classify into 4 types of domain classes: $x+$, $x-$, $y+$, and $y-$, each comprised of two types of domains. Denoting the directions $x \equiv [110]_p$, $y \equiv [1\bar{1}0]_p$, and $z \equiv [001]_p$, the order parameters in the 4 types of domain classes are $x+$: $(p_x, 0, 0, q_x, 0, 0)$ and $(p_x, 0, 0, -q_x, 0, 0)$; $x-$: $(-p_x, 0, 0, -q_x, 0, 0)$ and $(-p_x, 0, 0, q_x, 0, 0)$; $y+$: $(0, p_y, 0, 0, q_y, 0)$ and $(0, p_y, 0, 0, -q_y, 0)$; and $y-$: $(0, -p_y, 0, 0, q_y, 0)$ and $(0, -p_y, 0, 0, -q_y, 0)$. These domains are separated by $180°$ AFD (FE) domain walls across which **p** (**q**) remains the same, but **q** (**p**) rotates by $180°$, and $90°$ ($180°$) FE + AFD domain walls across which both **p** and **q** rotate by $90°$ ($180°$). In the pure FE phase, the order parameter **q** disappears, resulting in 4 types of domains and 2 types ($90°$ and $180°$) of ferroelectric domain walls.

We employ optical second harmonic generation (SHG) to study domain structures and phase transitions [14,15]. SHG involves the conversion of light (electric field E^ω) at a frequency ω into an optical signal at a frequency 2ω by a nonlinear medium, through the creation of a nonlinear polarization $P_i^{2\omega} \propto d_{ijk} E_j^\omega E_k^\omega$ [16]. The light source for SHG experiment was a Ti:sapphire laser with a pulse width of 140 femtoseconds, repetition rate of 1 kHz, and a
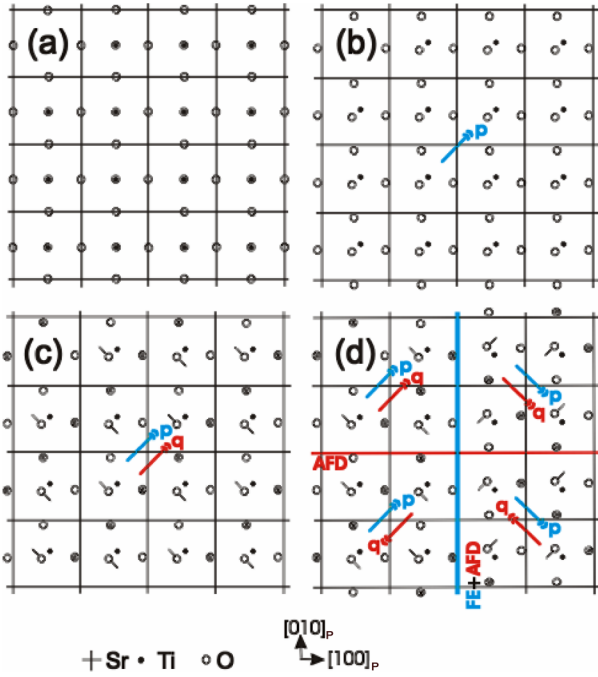
FIG. 1 (color online). Schematic showing Sr, O, and Ti atomic positions and order parameters **p** and **q** in various phases of strained SrTiO₃. (a) Paraelectric $4/mmm$ phase, (b) ferroelectric $mm2$ phase, (c) FE and AFD $mm2$ phase. Circles with crosses (dashes) are oxygen ions moving into the plane of the Letter (in the dash direction). (d) Domains in the FE + AFD phase showing an AFD and coupled FE + AFD domain wall.
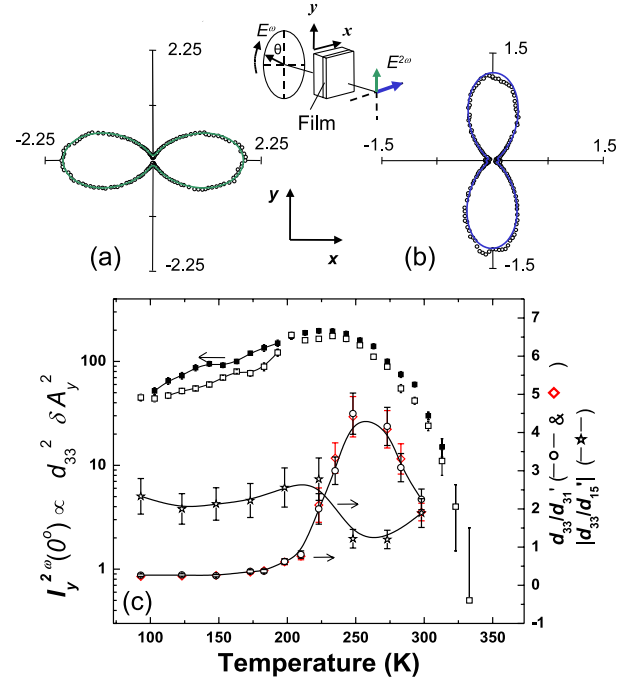

FIG. 2 (color online). (a),(b) Polar plots of SHG intensity $[I_j^{2\omega}(\theta)[$ at $T = 123$ K. (a) $I_y^{2\omega}$ and (b) $I_x^{2\omega}$, where directions $x \equiv [110]_p$ and $y \equiv [1\bar{1}0]_p$ are defined in the inset. The circles are the measured data, and the solid curves are the theoretical fits based on Eq. (1). (c) $I_y^{2\omega}(\theta = 0°)$ vs T where the dark (hollow) squares are the cooling (heating) cycle. The anomaly around 148 and 173 K are highlighted with spline curves. The variation of ratios of nonlinear optical coefficients with temperature is shown on the right axis. The circles (diamonds) represent $K_{3,y}$ ($K_{3,x}^{-1}$).

wavelength of 800 nm. A fundamental wave of 800 nm was incident from the substrate side in normal geometry. Its polarization direction, at an angle θ from the y axis, was rotated continuously within the plane of the film [see Fig. 1(a)]. The intensity $I_j^{2\omega}$ of the output SHG signal at 400 nm wavelength from the film was detected along either $j = x, y$ polarization directions by a photomultiplier tube. The resulting polar plots of the SHG intensity at 123 K are shown in Fig. 2. A reference study of a bare (110) DyScO₃ substrate without any film yielded no SHG intensity within the detection limits. Using SHG, the point group of this film at 223 K (ferroelectric phase) was determined to be $mm2$, and the ferroelectric polarization **p** was found to be along the $\langle 110 \rangle_p$ axes in the film plane [7], consistent with first principles calculations. A theoretical analysis of this film system yields the following expression for the SHG intensity [17]:

$$I_j^{2\omega} = K_{1,j}\sin^2 2\theta + K_{2,j}(\sin^2\theta + K_{3,j}\cos^2\theta)^2$$
$$+ K_{4,j}(\sin^2\theta + K_{3,j}\cos^2\theta)\sin 2\theta, \quad (1)$$

where $K_{i,j}$ are constants given by:

$$K_{3,x} = \frac{1}{K_{3,y}} = \frac{d_{31}'}{d_{33}}, \quad (2)$$

$$\left(\frac{1}{K_{3,y}}\right)^2 \left(\frac{K_{1,x}}{K_{2,x}}\frac{K_{1,y}}{K_{2,y}}\right) = \left(\frac{d_{15}'}{d_{33}}\right)^4, \quad (3)$$

$$\left(\frac{K_{1,x}K_{2,y}}{K_{2,x}K_{1,y}}\right)K_{3,y}^2 = \left(\frac{\delta A_y}{\delta A_x}\right)^4, \quad (4)$$

where $d_{31}' = (d_{31} + d_{32})/2$ and $d_{15}' = (d_{15} + d_{24})/2$. Two of these are ratios of nonlinear coefficients [d_{31}'/d_{33} (including its sign) and d_{15}'/d_{33} (absolute value only)] that are independent of domain microstructure. The third quantity, $\delta A_x/\delta A_y$, is a microstructural quantity, where $\delta A_x = A_{x+} - A_{x-}$ and $\delta A_y = A_{y+} - A_{y-}$ are the net area fractional biases in the x and y directions, respectively. The inverse relation between $K_{3,x}$ and $K_{3,y}$, stipulated by Eq. (2), can be seen to hold at all temperatures studied [Fig. 2(c)], showing that the symmetry is $mm2$ and the polarization is oriented along $\langle 110 \rangle_p$ directions in the 80–298 K range studied. These properties also show an anomaly in the range of $T_{\max} \sim 250$–273 K, consistent with the peak in the dielectric response ϵ reported in Ref. [8]. Noncentrosymmetry and polarization P_s exist well up to *at least* $T_b \sim 323$–328 K, where finally the SHG signal is below our detection limit. The SHG signal in Fig. 1(c) also

shows a reproducible anomaly at $T_{\text{AFD}} \sim 148$ K (cooling) to $T_{\text{AFD}} \sim 173$ K (heating). This corresponds to the anti-ferrodistortive phase transition in SrTiO$_3$, consistent with thermodynamic predictions [7,12]. The slight drop in the SHG intensity at the AFD transition could arise from doubling of the domain variants from 4 to 8 in the multiferroic phase or a change in the magnitude of d_{33} across the phase transition. The symmetry is observed to remain $mm2$ across the AFD transition, as predicted.
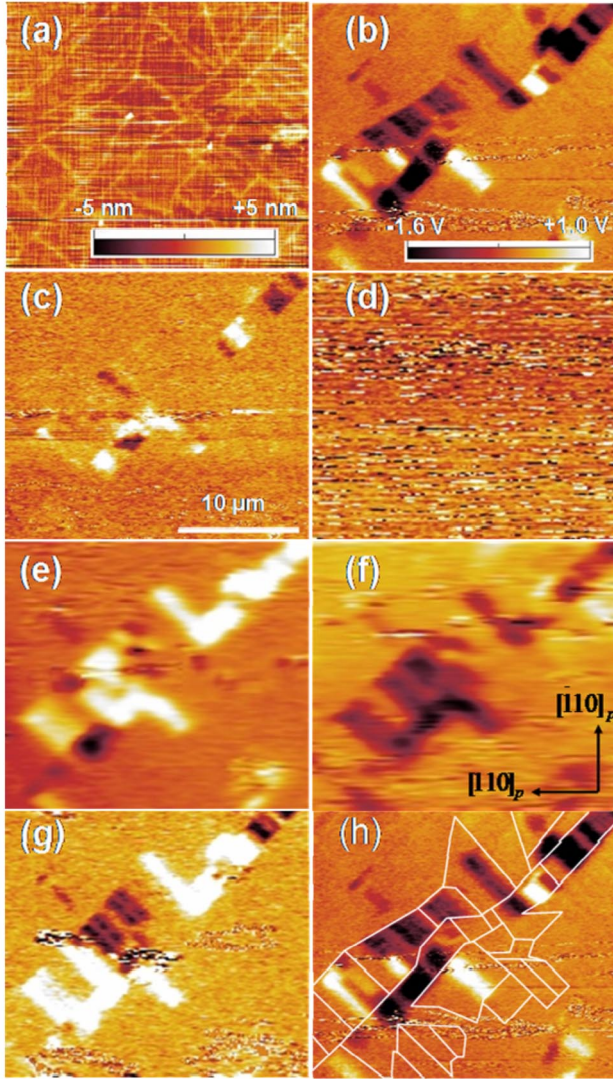

FIG. 3 (color online). Lateral PFM images of the same strained SrTiO$_3$ thin film. (a) Topography of the film surface. PFM image of the film (b) at room temperature, 298 K, (c) heated to 313 K, (d) heated to 333 K, and (e) cooled from 333 K back to room temperature. PFM response as the film was poled along $[110]_p$ with (f) +1 kV/mm and (g) −1 kV/mm. (h) PFM image of the film at room temperature. The white lines highlight the cracks in the film as seen from the topographic image. The color bar [inset (b)] applies to images [(b)–(g)] and the length scale [inset (c)], and the directions [inset (f)] apply to all panels.

The difference in the temperatures at which the peak in the dielectric constant and the peak in the d_{33}/d_{31}' ratio occurs ($T_{\text{max}} \sim 250$ K) versus where noncentrosymmetry was lost ($T_b \sim 323$ K) can arise from ferroelectric relaxor behavior as recently reported [18], as well as inhomogeneously strained regions. The $T_b \sim 323$–328 K transition may then be the Burns temperature [19]. Between T_{max} and T_b, polarization in a relaxor ferroelectric is normally expected to exist as glassy nanopolar regions without well-defined domains or domain walls. This is consistent with piezoelectric force microscopy (PFM) at room temperature (298 K), which reveals that the majority of the film is featureless with low piezoelectric signals. In the lateral PFM mode, $x\pm$ and $y\pm$ domains can be imaged as shown in Fig. 3(b). A shear strain ε_5 arising from the d_{15} coefficient will give lateral displacements in the x-z (y-z) planes in the $x\pm$ ($y\pm$) domains, giving different lateral contrasts between these domains [20]. Some localized regions (estimated to be in $\sim 5\%$ of the film area), however, reveal ferroelectric domains at room temperature as seen in Fig. 3(b), indicating slight inhomogeneity in strain. Upon heating, the piezoelectric response starts to disappear partially at 40 °C [Fig. 3(c)] and completely at 60 °C [Fig. 3(d)], and the domain features reappear on cooling [Fig. 3(e)] back to room temperature. The domains are partly bounded by ~ 5 nm high surface ridgelike features seen in topography [see Fig. 3(h)], within which they reappear after cooling [Fig. 3(e)]. Although these films have the narrowest dielectric constant versus temperature
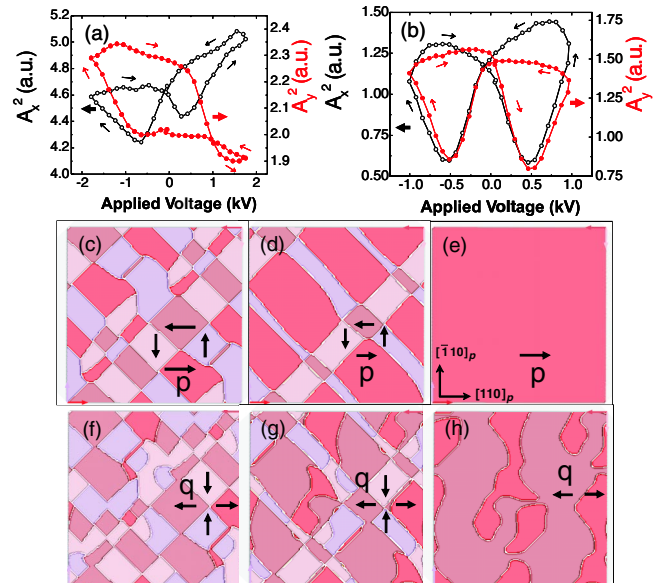

FIG. 4 (color online). Domain area fractions $[I_x^{2\omega}(0°) \propto \delta A_x^2$; $I_y^{2\omega}(0°) \propto \delta A_y^2]$ as a function of applied voltage along the $+x([110]_p)$ direction at (a) $T = 123$ K and (b) $T = 223$ K. Phase-field modeling of the evolution of FE [(c)–(e)] and AFD [(f)–(h)] domain morphologies with electric field along $x([110]_p)$.

peaks reported for $SrTiO_3$ or $(Ba, Sr)TiO_3$ films [18], the widths are still about 3 times broader than $(Ba, Sr)TiO_3$ single crystals [21]; hence, local inhomogeneous strains and domains can arise.

The bright and dark regions of the PFM signal in Fig. 3(b) can be attributed to the $y\pm$ and $x\pm$ domains, respectively. The domain walls [not related to topography; see Fig. 3(h)] separating these bright and dark domains are parallel to the $\langle 100 \rangle_p$ direction, which correspond to 90° domain walls. These walls can be influenced by external electric fields. Figure 3(e) shows that cooling has produced predominantly $y\pm$ domains. Two gold pads, 1000 Å thick and 1.3 mm apart, were sputtered on the film in its plane such that an external electric field could be applied along the $\pm x[110]_p$ direction. When an electric field of $+1$ kV/mm is applied along the $+x$ direction, they transform to predominantly $x\pm$ domains [Fig. 3(f)] and then partially reverse back to $y\pm$ domains after applying -1 kV/mm along the $-x$ direction [Fig. 3(g)]. These results indicate 90-degree ferroelectric domain wall motion. Figures 4(a) and 4(b) show that both δA_x^2 and δA_y^2 change in response to an electric field of ± 1 kV applied across the gap. This indicates that the electric field along the $\pm x$ direction switches domains along the $\pm y$ direction as well, indicating motion of 90° domain walls that couple $x\pm$ domains to the $y\pm$ domains. This mechanism is operative at all temperatures including the multiferroic phase, where SHG indicates the motion of coupled 90° ferroelectric-ferroelastic domain walls.

Phase-field simulations [7] in the multiferroic phase [Figs. 4(c)–4(h)] clearly show that, under an electric field, the area fraction of $x+$ domains increases, while that of $x-$ domains decreases through a motion of coupled 90° ferroelectric-ferroelastic domain walls. The pure 180° AFD walls [see Fig. 1(d)] within a single polarization domain state are degenerate in energy even under an electric field and remain with statistically equal populations [Figs. 4(f)–4(h)]. The pure AFD domain walls within the polarization domain states not favored by the external field disappear, however, primarily as the 90° walls sweep through that domain state.

In conclusion, a unique form of multiferroicity, namely, an induced ferroelectric-antiferrodistortive phase in strained $SrTiO_3$, is reported. For the first time, ferroelectric domains were directly imaged at room temperature and above in this material using PFM. *In situ* SHG under external fields show evidence for the movement of coupled ferroelectric-ferroelastic 90° domain walls in the multiferroic phase, in agreement with phase-field modeling. From a symmetry perspective, the domain structure and

dynamics in this ferroelectric-antiferrodistortive system could have relevance to expected domain structures in a ferroelectric-(anti)ferromagnetic system with two phase transitions.

*Electronic address: vgopalan@psu.edu

[1] N. A. Spaldin and M. Fiebig, Science **309**, 391 (2005).

[2] M. Fiebig, J. Phys. D **38**, R123 (2005).

[3] W. Eerenstein, N. D. Mathur, and J. F. Scott, Nature (London) **442**, 759 (2006).

[4] K. A. Muller and H. Burkard, Phys. Rev. B **19**, 3593 (1979).

[5] A. Antons, J. B. Neaton, K. M. Rabe, and D. Vanderbilt, Phys. Rev. B **71**, 024102 (2005).

[6] N. A. Pertsev, A. G. Zembilgotov, and A. K. Tagantsev, Phys. Rev. Lett. **80**, 1988 (1998).

[7] Y. L. Li *et al.*, Phys. Rev. B **73**, 184112 (2006).

[8] J. H. Haeni *et al.*, Nature (London) **430**, 758 (2004).

[9] H. Unoki and T. Sakudo, J. Phys. Soc. Jpn. **23**, 546 (1967).

[10] J. C. Slonczewski and H. Thomas, Phys. Rev. B **1**, 3599 (1970).

[11] K. A. Müller, W. Berlinger, and F. Waldner, Phys. Rev. Lett. **21**, 814 (1968).

[12] J. Wang *et al.*, Science **299**, 1719 (2003).

[13] F. He, B. O. Wells, and S. M. Shapiro, Phys. Rev. Lett. **94**, 176101 (2005).

[14] V. Gopalan and R. Raj, J. Appl. Phys. **81**, 865 (1997).

[15] M. Fiebig, V. V. Pavlov, and R. V. Pisarev, J. Opt. Soc. Am. B **22**, 96 (2005).

[16] Y. R. Shen, *The Principles of Nonlinear Optics* (Wiley, New York, 2003), p. 86.

[17] A. Sharan, J. Lettieri, Y. Jia, W. Tian, X. Pan, D. G. Schlom, and V. Gopalan, Phys. Rev. B **69**, 214109 (2004).

[18] M. D. Biegalski, Y. Jia, D. G. Schlom, S. Trolier-McKinstry, S. K. Streiffer, V. Sherman, R. Uecker, and P. Reiche, Appl. Phys. Lett. **88**, 192907 (2006).

[19] G. Burns and F. H. Dacol, Solid State Commun. **48**, 853 (1983).

[20] D. A. Scrymgeour and V. Gopalan, Phys. Rev. B **72**, 024103 (2005).

[21] K. Bethe and F. Welz, Mater. Res. Bull. **6**, 209 (1971).